
Non-saturating GAN training as divergence minimization

Matt Shannon
Eric Battenberg

Ben Poole
David Kao
Google, Mountain View, California, USA

Soroosh Mariooryad
Daisy Stanton

Tom Bagby
RJ Skerry-Ryan

Abstract

Non-saturating generative adversarial network (GAN) training is widely used and has continued to obtain groundbreaking results. However so far this approach has lacked strong theoretical justification, in contrast to alternatives such as f-GANs and Wasserstein GANs which are motivated in terms of approximate divergence minimization. In this paper we show that non-saturating GAN training does in fact approximately minimize a particular f-divergence. We develop general theoretical tools to compare and classify f-divergences and use these to show that the new f-divergence is qualitatively similar to reverse KL. These results help to explain the high sample quality but poor diversity often observed empirically when using this scheme.

1 Introduction

Generative adversarial networks (GANs) (Goodfellow et al., 2014) have enjoyed remarkable progress in recent years, producing images of striking fidelity, resolution and coherence (Karras et al., 2018; Miyato et al., 2018; Brock et al., 2018; Karras et al., 2019). A GAN consists of two components: a *generator* produces a synthetic image (for example) and a *critic* or *discriminator* aims to distinguish these synthetic images from natural ones. The generator and critic are trained adversarially to try to outwit each other, thus improving the generator. There has been recent progress in both theoretical and practical aspects of understanding and performing GAN training (Nowozin et al., 2016; Arjovsky and Bottou, 2017; Arjovsky et al., 2017; Mescheder et al., 2018; Gulrajani et al., 2017; Sønderby et al., 2017; Miyato et al., 2018; Karras et al., 2018; Brock et al., 2018; Karras et al., 2019).

A rich vein of developments has come from viewing GAN training as *divergence minimization*. The discrepancy between the data distribution and the distri-

bution of generator output is measured by a probabilistic divergence. The critic has an ancillary role, allowing this divergence to be tractably estimated and minimized. Conventional GAN training approximately minimizes the Jensen-Shannon divergence (Goodfellow et al., 2014), f-GANs (Nowozin et al., 2016) approximately minimize f-divergences such as reverse KL, and Wasserstein GANs (Arjovsky et al., 2017) approximately minimize the Wasserstein-1 metric.

Despite these theoretically well-founded developments, one of the most widely used GAN training methods is a heuristic *non-saturating* scheme (Goodfellow et al., 2014). This modifies the original Jensen-Shannon-based generator gradient to provide a stronger learning signal early in training. This approach has continued to obtain groundbreaking results (Karras et al., 2019) and outperformed other GAN variants on some tasks in a recent systematic comparison (Lucic et al., 2018).

The main result of this paper is that the non-saturating scheme approximately minimizes the f-divergence $\text{KL}(\frac{1}{2}p + \frac{1}{2}q \| p)$, which we call the *softened reverse KL* (§3.2). This puts the non-saturating scheme on a similar footing to Wasserstein GANs as a principled approach with strong empirical results.

Our second major contribution is a set of general tools to compare f-divergences. We show how to write f-divergences in a way that allows easy visual comparison of their qualitative properties (§4.2), and develop a formulation of *tail weight* which generalizes the notions of *mode-seeking* and *covering* behavior (§4.3).

We use these general tools to show that softened reverse KL is mode-seeking and is qualitatively similar to reverse KL (§5.1), helping to explain the high sample quality but poor sample diversity of most GAN models trained with the non-saturating scheme.

Our final major contribution is to clarify the substantial confusion and conflicting claims in previous literature on theoretical aspects of non-saturating training (§5.3).

2 f-GAN training

In this section we review f-GAN training (Nowozin et al., 2016). We use a slightly modified formulation, presented in detail in a technical report (Shannon, 2020), which ensures that the optimal critic is the same for all f-divergences and avoids having to worry about various small details such as the domains of Fenchel conjugates (Nowozin et al., 2016). Throughout the paper we use the convention that p is the “true” distribution and the *generator* distribution q is a model intended to approximate p .

2.1 f-GAN formulation

Given a strictly convex twice continuously differentiable function $f : \mathbb{R}_{>0} \rightarrow \mathbb{R}$ with $f(1) = f'(1) = 0$, the *f-divergence* (Csiszár, 1967; Ali and Silvey, 1966) between probability distributions with densities p and q over \mathbb{R}^K is defined as

$$D_f(p, q) = \mathbb{E}_{x \sim q} \left[f \left(\frac{p(x)}{q(x)} \right) \right] \quad (1)$$

For simplicity, we assume the probability distributions p and q are suitably nice, e.g. absolutely continuous with respect to the Lebesgue measure on \mathbb{R}^K , $p(x), q(x) > 0$ for $x \in \mathbb{R}^K$, and p and q continuously differentiable.¹ We refer to f as the *defining function* of the divergence D_f . The constraint $f'(1) = 0$ removes an irrelevant degree of freedom and is not a restriction (Shannon, 2020). Since $f(1) = f'(1) = 0$, f'' completely determines f . Working in terms of f'' is convenient since f'' has a simpler algebraic form than f for many common f-divergences.

An f-divergence has a simple variational lower bound based on bounding f by its tangent lines (Nowozin et al., 2016; Shannon, 2020). For any continuously differentiable function $d : \mathbb{R}^K \rightarrow \mathbb{R}$, we have

$$D_f(p, q) \geq E_f(p, q, d)$$

with equality iff $d = d^*$, where

$$E_f(p, q, d) = \mathbb{E}_{x \sim p} [a_f(d(x))] - \mathbb{E}_{x \sim q} [b_f(d(x))] \quad (2)$$

$$d^*(x) = \log p(x) - \log q(x) \quad (3)$$

and $a_f, b_f : \mathbb{R} \rightarrow \mathbb{R}$ are defined by

$$a_f(\log u) = f'(u) \quad (4)$$

$$b_f(\log u) = u f'(u) - f(u) \quad (5)$$

¹The constraint $q(x) > 0$ is often violated in practice due to the GAN generator taking a low-dimensional random input to produce a high-dimensional output. We advocate injecting noise at all levels of the generator network including the output (Shannon, 2020). This can have advantages in practice (Karras et al., 2019).

The *critic* or *discriminator* d approximates the log density ratio between p and q .

Typically the generator distribution and critic are both parameterized. The critic is parameterized directly as a neural net d_ν with parameters ν . The generator distribution is specified implicitly: noise z sampled from a fixed distribution is passed through a neural net g_λ with parameters λ and the output $g_\lambda(z)$ is taken as a sample from q_λ . The value $E_f(p, q_\lambda, d_\nu)$ and its gradient with respect to the critic parameters ν can be approximated using samples from p and q_λ . To compute the gradient with respect to the generator parameters λ , it is helpful to “reparameterize” the expectation over q in (2) to obtain (Kingma and Welling, 2014)

$$E_f(p, q_\lambda, d) = -\mathbb{E}_z [b_f(d(g_\lambda(z)))] + \text{const} \quad (6)$$

Training of the (critic, generator) system is inherently adversarial, since obtaining an accurate estimate of $D_f(p, q_\lambda)$ requires maximizing the lower bound $E_f(p, q_\lambda, d_\nu)$ with respect to ν , but overall we want to minimize $D_f(p, q_\lambda)$ with respect to λ . Typically both λ and ν are updated using a gradient-based optimizer such as SGD, ADAM or RMSProp, with a single generator update performed after or simultaneously with one or more critic updates.

Convergence of GAN training algorithms is still a complicated topic despite much attention (Nagarajan and Kolter, 2017; Gulrajani et al., 2017; Kodali et al., 2017; Mescheder et al., 2017, 2018; Fedus et al., 2018; Balduzzi et al., 2018; Peng et al., 2019, for example). The definition of $E_f(p, q_\lambda, d)$ ensures that, in the case where the critic d is unrestricted, the only fixed points of training dynamics are at $(\lambda, d) = (\lambda^*, 0)$ for λ^* a stationary point of $\lambda \mapsto D_f(p, q_\lambda)$. These fixed points are often Nash equilibria and locally stable (Nagarajan and Kolter, 2017; Mescheder et al., 2018). The gradient matching property described in §2.2 shows that performing very many critic updates from scratch for each generator update, but not so many as to overfit, essentially performs gradient descent on D_f , and so will find a local minimum in D_f . However in practice the critic will always be somewhat suboptimal and the generator updates will not follow the gradient of D_f exactly (see §A for a simple example). The restricted parametric form of the critic may also lead to suboptimal fixed points. Because of the issues with parameterization and optimization of the critic, we refer to f-GAN training as *approximate* divergence minimization.

The three main f-divergences we consider are:

- The Kullback-Leibler (KL) divergence $\text{KL}(p \parallel q)$. This has $f''(u) = u^{-1}$, $a'_f(d) = 1$ and $b'_f(d) = \exp d$.

- The reverse KL divergence $\text{KL}(q \parallel p)$. This has $f''(u) = u^{-2}$, $a'_f(d) = \exp(-d)$ and $b'_f(d) = 1$.
- The canonicalized (see §2.2) Jensen-Shannon divergence $4\text{JS}(p, q) = 2\text{KL}(p \parallel m) + 2\text{KL}(q \parallel m)$ where $m = \frac{1}{2}p + \frac{1}{2}q$. This has $f''(u) = \frac{2}{u(u+1)}$, $a'_f(d) = 2\sigma(-d)$ and $b'_f(d) = 2\sigma(d)$, where σ is the logistic sigmoid function $\sigma(d) = 1/(1 + \exp(-d))$.

2.2 Properties of f-GAN training

In this section we describe three properties of f-GAN training which are relevant to our discussion of the non-saturating loss in §3 and §5.

Different f-divergences may behave very differently when p and q are far apart but are essentially identical when p is close to q : if $p \approx q$ then $D_f(p, q) \approx f''(1)\text{KL}(p \parallel q)$ to second order (Sason and Verdú, 2016; Shannon, 2020). The factor $f''(1)$ represents an overall scale factor which is often not important, and so we typically scale f-divergences to have $f''(1) = 1$, which we refer to as *canonical* form. Thus all canonical f-divergences agree when p is close to q .

The variational lower bound E_f satisfies a convenient gradient matching property not mentioned by Nowozin et al. (2016). We have already seen that the values of E_f and D_f match when the critic is optimal. The same is true of the generator gradient:

$$\frac{\partial}{\partial \lambda} D_f(p, q_\lambda) = \frac{\partial}{\partial \lambda} E_f(p, q_\lambda, d) \Big|_{d=d_\lambda^*} \quad (7)$$

This can be derived from E_f being a tight lower bound or directly from the definition of E_f (Shannon, 2020). Goodfellow et al. (2014, Section 4.2) described this property for the specific case of Jensen-Shannon. Wasserstein GANs satisfy a similar property (Arjovsky et al., 2017). As far as we are aware, this result is novel for general f-GANs. The gradient matching property shows that the best estimate of the generator gradient for a given λ is obtained by having as well-trained a critic as possible. Any weak generator gradient when using a strong critic is due to the original f-divergence having a weak gradient (e.g. Jensen-Shannon).

There is a simple generalization of the above training procedure, which is to base the generator gradient on E_f but the critic gradient on E_h for a possibly different defining function h (Poole et al., 2016, Section 2.3). We refer to this as a *hybrid* (f, h) f-GAN training scheme. The optimal critic for h is the same as the optimal critic for f . Therefore, in the case where the critic d is unrestricted, the only fixed points of training dynamics are again at $(\lambda, d) = (\lambda^*, 0)$ for λ^* a stationary point of $\lambda \mapsto D_f(p, q_\lambda)$. The same argument

about behavior in the limit of a large number of critic updates per generator update also applies. Thus a hybrid (f, h) scheme may be interpreted as minimizing D_f , the divergence used for updating the *generator*.

3 Non-saturating GAN training

In practice the original generator gradient based on the Jensen-Shannon divergence performs poorly, and typically an alternative *non-saturating* generator gradient is used instead (Goodfellow et al., 2014). In this section we briefly review the issue with the original generator gradient, describe the non-saturating fix, and establish our main result relating non-saturating training to hybrid f-GAN training.

3.1 Non-saturating training procedure

Early on in training, the generator and data distribution are typically not well matched, with samples from p being very unlikely under q and vice versa. This means most of the probability mass of p and q is in regions where d has large magnitude (corresponding to the positive and negative tails in Figure 2 and (15) below). In this regime Jensen-Shannon essentially saturates at its maximum value, and it is not too surprising that this might lead to optimization issues. Similar concerns do not apply to other f-divergences such as KL or reverse KL, but an alternative “non-saturating” generator gradient has still been suggested for f-GANs (Nowozin et al., 2016). For both GANs and f-GANs the specific change is to replace b_f by a_f when computing the generator gradient using (6), that is to use

$$E_f(p, q_\lambda, d) = -\mathbb{E}_z [a_f(d(g_\lambda(z)))] + \text{const} \quad (8)$$

In the case of canonicalized Jensen-Shannon (i.e. conventional non-saturating GAN training) this means replacing $b_f(d) = -2\log\sigma(-d) - 2\log 2$ with $a_f(d) = 2\log\sigma(d) + 2\log 2$. We are not aware of a particular motivation for this procedure in the case of f-GANs other than that it yields the traditional non-saturating GAN scheme in the case of Jensen-Shannon.

3.2 Equivalence to hybrid f-GAN training

We now establish our main result: for any f-divergence D_h , “non-saturating” training based on h is precisely equivalent to a hybrid (f, h) scheme for some defining function f . This shows that the non-saturating scheme is not simply a trick to get a useful gradient, but entirely changes the divergence minimized by training.

Given h , we seek a defining function f such that $b'_f = a'_h$, since then the original generator gradient based on f obtained by differentiating (6) will be equal to the

“non-saturating” generator gradient based on h obtained by differentiating (8). Since $a'_h(\log u) = uh''(u)$ and $b'_f(\log u) = u^2 f''(u)$, there is only one possibility:

$$f''(u) = u^{-1} h''(u) \quad (9)$$

This defines a valid f-divergence since $f''(u) > 0$ and satisfies $b'_f = a'_h$ as desired. Since the critic gradient is still based on h , the overall scheme is a hybrid (f, h) one, and so approximately minimizes D_f .

We now explicitly compute the corresponding f for some common choices of h :

- For the KL divergence, $h''(u) = u^{-1}$, so $f''(u) = u^{-2}$. We already saw in §2.1 that this is the reverse KL divergence. Thus “non-saturating” training based on the KL divergence is a hybrid (reverse KL, KL) scheme, and so in fact approximately minimizes the reverse KL. This equivalence also follows directly from the equality of KL’s a_h to reverse KL’s b_f .
- For the reverse KL divergence, $h''(u) = u^{-2}$, so $f''(u) = u^{-3}$. Integrating twice to obtain f , this corresponds to the canonicalized Neymann χ^2 divergence $D_f(p, q) = \frac{1}{2} \int (q(x) - p(x))^2 / p(x) dx$.
- For the canonicalized Jensen-Shannon divergence, $h''(u) = \frac{2}{u(u+1)}$, so $f''(u) = \frac{2}{u^2(u+1)}$. Integrating twice to obtain f , this corresponds to $D_f(p, q) = 4 \text{KL}(\frac{1}{2}p + \frac{1}{2}q \| p)$.

The divergence $4 \text{KL}(\frac{1}{2}p + \frac{1}{2}q \| p)$ does not have an existing name as far as we are aware. In this paper we have termed it the *softened reverse KL (SRKL)*. The naming is explained in §E. It has $a'_f(d) = 2 \exp(-d) - 2\sigma(-d)$ and $b'_f(d) = 2\sigma(-d)$. Thus the non-saturating training scheme described by Goodfellow et al. (2014) is a hybrid (SRKL, JS) scheme, and so approximately minimizes the softened reverse KL.

In §A we validate our mathematical conclusions by training a GAN for which the evolution of the generator parameters can be directly observed. As expected, conventional saturating GAN training converges to a minimum of the Jensen-Shannon divergence and non-saturating GAN training converges to a minimum of the softened reverse KL.

4 Tools to compare f-divergences

Having established that non-saturating GAN training approximately minimizes the softened reverse KL divergence, we focus on understanding the qualitative properties of this divergence. In this section we develop analytic tools applicable to any f-divergence. We apply these tools to the softened reverse KL in §5.1.

4.1 Left and right mismatches

We start by developing a more symmetric representation of f-divergences. The definition (1) appears to be quite asymmetric in how it treats p and q , but it obeys a particular symmetry (Reid and Williamson, 2011). Define the *Csiszár dual* f_R by $f_R(u) = uf(u^{-1})$. Then $f'_R(u) = f(u^{-1}) - u^{-1}f'(u^{-1})$ and so $f''_R(u) = u^{-3}f''(u^{-1})$. It is easy to verify that $D_{f_R}(p, q) = D_f(q, p)$. With $A = \{x : q(x) > p(x)\}$ and $B = \{x : q(x) < p(x)\}$, we have

$$D_f(p, q) = \int_A q(x) f\left(\frac{p(x)}{q(x)}\right) dx + \int_B p(x) f_R\left(\frac{q(x)}{p(x)}\right) dx \quad (10)$$

This is more explicitly symmetric than (1) in the role of p and q . We refer to A as the set of *left mismatches* and B as the set of *right mismatches*. At each point in A , the model assigns higher density than the data, and the penalty paid for this mismatch in terms of the overall divergence D_f is governed by the behavior of $f(u)$ for $0 < u < 1$ (the “left” of the graph of f). Similarly the penalty paid for right mismatches, where the model assigns lower density than the data, is governed by $f(u)$ for $u > 1$. Note from (10) that a left mismatch can only be heavily penalized if the point is plausible under q , i.e. $q(x)$ is not tiny. Similarly a right mismatch can only be heavily penalized for points plausible under p .

4.2 Pushforwards and symmetry-preserving divergence plots

While the f-divergence framework unifies many divergences, just plotting the defining function f is often not informative. The symmetric relationship between divergences such as KL and reverse KL is obfuscated, and f may grow quickly even when the divergence is well-behaved. In this section we develop a straightforward and intuitive way to visually compare f-divergences.

Firstly note that for $x \sim q$, $d^*(x) = \log p(x) - \log q(x)$ is a random variable with some density $\tilde{q}(d)$ for $d \in \mathbb{R}$. Formally \tilde{q} is the *pushforward measure* of q through the function d^* . We can rewrite (1) as

$$D_f(p, q) = \mathbb{E}_{d \sim \tilde{q}} [f(\exp d)] \quad (11)$$

As above this can be written more symmetrically. Let

$$s_f(d) = \begin{cases} f(\exp d), & d < 0 \\ f_R(\exp(-d)) = \frac{f(\exp d)}{\exp d}, & d > 0 \end{cases} \quad (12)$$

By considering expectation of an arbitrary function of d expressed in x -space and d -space, we can show that

$$\tilde{q}(d) = \tilde{p}(d) \exp(-d) \quad (13)$$

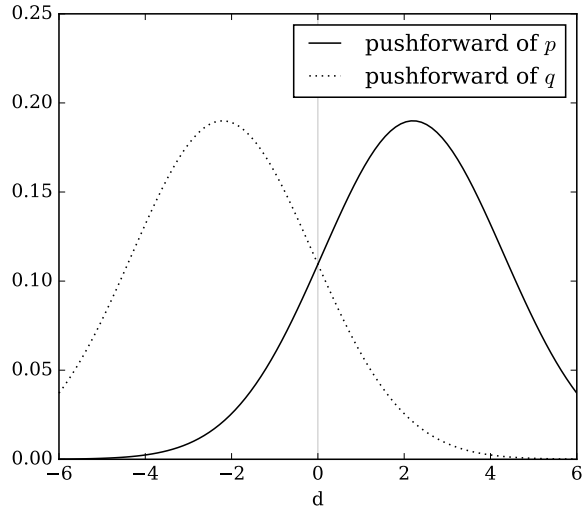


Figure 1: Plots of the pushforward densities $\tilde{p}(d)$ and $\tilde{q}(d)$ for the case where p and q are multidimensional Gaussians with common covariance. The f-divergence $D_f(p, q)$ may be obtained by integrating these pushforwards against s_f (e.g. Figure 2) using (15).

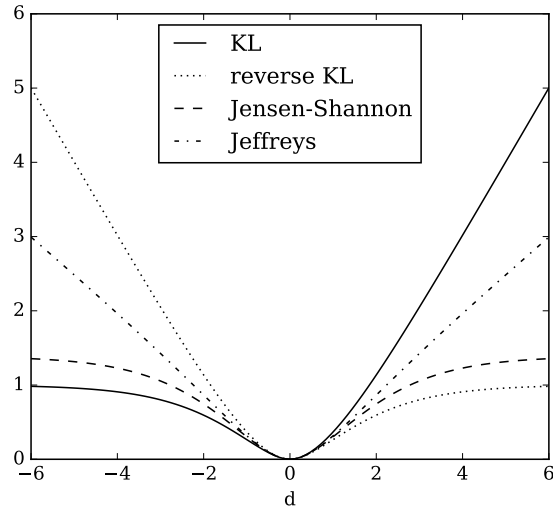


Figure 2: Plots of $s_f(d)$ for various f-divergences. The f-divergence $D_f(p, q)$ may be obtained by integrating s_f against their pushforwards (e.g. Figure 1) using (15). The symmetry between KL and reverse KL is evident.

where \tilde{p} is the pushforward of p through d^* . Thus, using (10) and (13), we can write the f-divergence as

$$D_f(p, q) = \int_{-\infty}^0 \tilde{q}(d) s_f(d) dd + \int_0^{\infty} \tilde{p}(d) s_f(d) dd \quad (14)$$

$$= \int_{-\infty}^{\infty} \max\{\tilde{p}(d), \tilde{q}(d)\} s_f(d) dd \quad (15)$$

where the last equality follows from (13) since $\tilde{q}(d)$ is larger than $\tilde{p}(d)$ for $d < 0$ and vice versa for $d > 0$.

Examples of pushforwards for the simple case where p and q are multidimensional Gaussians with common covariance are shown in Figure 1. In this case the pushforwards \tilde{q} and \tilde{p} are themselves one-dimensional Gaussians (since d^* is linear), with densities $\mathcal{N}(-\frac{1}{2}\sigma^2, \sigma^2)$ and $\mathcal{N}(\frac{1}{2}\sigma^2, \sigma^2)$ respectively, for some σ (this follows from (13)). Examples of s_f for various f-divergences are shown in Figure 2. We refer to s_f as a *symmetry-preserving* representation of f . Note that s_f is twice continuously differentiable at zero (using $f'(1) = 0$).

An f-divergence $D_f(p, q)$ involves an interaction between the distributions p, q and the defining function f , and (15) nicely decomposes this interaction in terms of something that only depends on p and q (the pushforwards) and something that only depends on f (the function s_f), connected via a one-dimensional integral. By plotting the pushforwards, we can get a feel for what types of mismatch between p and q are present in multidimensional x -space, and understand at a glance how badly these mismatches would be penalized for a

given f-divergence. By plotting s_f and imagining integrating against various pushforwards, we can see the properties of different f-divergences in a very direct way. For example, Figure 2 directly expresses several facts about divergences. It shows that left mismatches (regions of space where $q(x) > p(x)$, corresponding to $d < 0$) are penalized by reverse KL much more severely than right mismatches (regions of space where $q(x) < p(x)$, corresponding to $d > 0$). The symmetry between KL and reverse KL is evident. We see that Jensen-Shannon and the Jeffreys divergence (the arithmetic mean of KL and reverse KL) are both symmetric in how they penalize left and right mismatches, but differ greatly in how much they penalize small versus large mismatches.

4.3 Classification of f-divergence tails

In this section we introduce a classification scheme for f-divergences in terms of their behavior for large left and right mismatches. These *tail weights* determine many aspects of an f-divergence's qualitative behavior.

First we define the notion of tail weight and examine some of its consequences. We write $g(u) \sim h(u)$ as $u \rightarrow a$ to mean $g(u)/h(u) \rightarrow 1$ as $u \rightarrow a$. If $f''(u) \sim Cu^{-L}$ as $u \rightarrow 0$ and $f''(u) \sim Du^{R-3}$ as $u \rightarrow \infty$ where $C, D > 0$ then we say that D_f has (Cu^{-L}, Du^{R-3}) tails and (L, R) tail weights. Note that, since $f''_R(u) = u^{-3}f''(u^{-1})$ (see §4.1), f having a u^{R-3} right tail is equivalent to f_R having a u^{-R} left tail. Thus tail weights interact simply with symmetry: if $D_f(p, q)$ has (L, R) tail weights then

divergence	(left, right) tail weights	bounded?
KL	(1, 2)	no
RKL	(2, 1)	no
Jensen-Shannon	(1, 1)	yes
Jeffreys	(2, 2)	no
Neymann χ^2	(3, 0)	no
softened RKL	(2, 0)	no
IGOG	(2, 0)	no

Table 1: Tail weights and boundedness for the f-divergences considered in this paper. A divergence is bounded if and only if the left and right tail weights are both less than 2.

$D_{f_R}(p, q) = D_f(q, p)$ has (R, L) tail weights. Intuitively, the left tail weight L determines how strongly large left mismatches are penalized compared to small mismatches (which are penalized the same amount by every canonical f-divergence), whereas the right tail weight R determines how strongly large right mismatches are penalized compared to small mismatches.

Some f-divergences such as Jensen-Shannon are bounded, meaning there is an $M \in \mathbb{R}$ such that $D_f(p, q) \leq M$ for all densities p and q , while others such as KL are unbounded. We show in §C that tail weights determine boundedness: a divergence is bounded iff $L, R < 2$. Furthermore D_f is bounded iff s_f is bounded, so we can visually see boundedness on symmetry-preserving divergence plots such as Figure 2. The tail weights and boundedness properties of various f-divergences are summarized in Table 1.

Tail weights provide an extension of the typical classification of divergences as *mode-seeking* or *covering* (Bishop, 2006, Section 10.1.2). Models trained with reverse KL tend to have distributions which are more “compact” or “localized” than the true distribution, sometimes only successfully modeling certain modes (density peaks) of a multi-modal true distribution. Models trained with KL tend to have distributions which are less compact than the true distribution, “covering” the true distribution entirely even if it means putting density in regions which are very unlikely under the true distribution (Bishop, 2006, Figure 10.3). However there are important qualitative aspects of divergence behavior that are not captured by these labels. For example, Jensen-Shannon and the Jeffreys divergence are both neither mode-seeking nor covering, but have very different behavior from each other. Tail weights capture these distinctions in a straightforward but precise way.

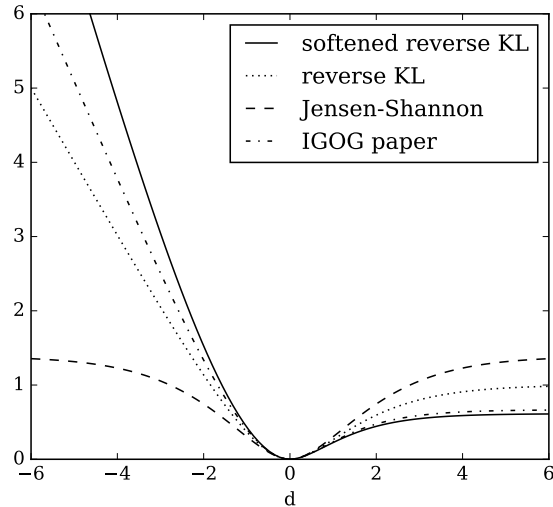


Figure 3: Plots of $s_f(d)$ for various reverse KL-like f-divergences and Jensen-Shannon. Softened reverse KL is the divergence effectively minimized by non-saturating GAN training. IGOG is the divergence derived by Poole et al. (2016).

5 Discussion

In this section we apply the tools developed in §4 to understand the qualitative behavior of the softened reverse KL divergence, discuss the relationship between our results and previous attempts to analyze non-saturating GAN training theoretically, and outline ways the perspectives and tools developed in the paper may be useful in practice.

5.1 Qualitative properties of softened RKL

In this section we apply the tools developed in §4 to analyze the properties of the softened reverse KL divergence minimized by non-saturating GAN training.

Figure 3 shows the symmetry-preserving representation $s_f(d)$ for Jensen-Shannon and softened reverse KL, as well as the reverse KL for comparison. The qualitative behavior of softened reverse KL is quite similar to reverse KL. The softened version has a steeper slope in the roughly linear left tail and changes the right tail behavior slightly, but these are relatively minor differences. Jensen-Shannon is extremely different to reverse KL and softened reverse KL.

Tail weights and boundedness provide a very concise way to see the qualitative behavior of non-saturating GAN training. The softened reverse KL divergence has tail weights $(2, 0)$, and so is unbounded, is likely to have a strong gradient starting from a random initialization where large mismatches are present, and penalizes left mismatches strongly but tolerates large

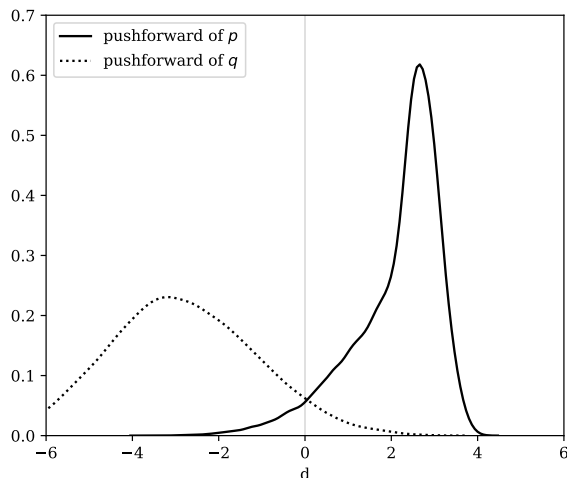


Figure 4: Pushforward plot for StyleGAN (Karras et al., 2019). This shows the histogram of the critic output value on real and fake images. We can see that the critic is easily able to distinguish real and fake images most of the time, but we do not see substantial mode-seeking or covering behavior.

right mismatches and so is mode-seeking. In contrast the Jensen-Shannon divergence approximately minimized by saturating GAN training has tail weights (1, 1), and so is bounded, is likely to have a weak gradient in the presence of large mismatches, and tolerates large left and right mismatches.

5.2 Empirical pushforward plots

In §4.2 we described pushforward plots obtained by pushing the distributions p and q through the optimal critic d^* . This is easy to approximate empirically, using the learned critic instead of the optimal critic, by plotting the histogram of the critic output $d(x)$ for real and fake x . Critic output histograms were previously investigated by Grewal et al. (2017, Figure 1). StyleGAN (Karras et al., 2019) is a recent high-quality image generation GAN trained with the non-saturating training scheme modified with a gradient penalty. Its pushforward plot is shown in Figure 4.² From this plot we can read off the prevalence of different severities of left and right mismatch, as well as compute the approximate value of any f-divergence. Here we do not see substantial mode-seeking or covering: there are no heavy left or right tails (as in Figure 6 and Figure 7), and no separate peaks at large negative or positive values of d (as in Figure 8 and Figure 10). More examples of pushforward plots are given in §D.

²Pre-trained model `stylegan-ffhq-1024x1024.pkl` available at <https://github.com/NVlabs/stylegan>. The critic was trained for a further 6000 examples while keeping the (non-moving-average) generator fixed.

5.3 Previous discussion of non-saturating scheme

The training dynamics of the non-saturating scheme and whether it can be motivated in a principled way have been a source of discussion and some confusion. In this section we review previous attempts to view non-saturating GAN training as a form of divergence minimization.

Goodfellow et al. (2014, Section 3) claim that, compared to the saturating training scheme based on the Jensen-Shannon divergence, the non-saturating training scheme “results in the same fixed point of the dynamics of G and D but provides much stronger gradients early in learning.” It is true that the original and non-saturating generator gradients give the same final result in the non-parametric case where q is unrestricted, but this is fairly trivial since both gradients lead to $q = p$, as do all divergences. It is even true that the dynamics of training are essentially the same for the original and non-saturating gradients when $q \approx p$, but again this is fairly trivial since all f-divergences agree in this regime, as discussed in §2.2. However the “fixed point of the dynamics” is certainly not the same in the general case of parametric q with some model mismatch (see §A for an empirical demonstration). Our results provide a precise way to view the relationship between saturating and non-saturating generator gradients: they are optimizing different f-divergences.

Nowozin et al. (2016, Section 3.2)³ present a simple argument that the “non-saturating” f-GAN training scheme has the same fixed points and that the original and non-saturating generator gradients have the same direction. However this argument is erroneous. It is true that if $p \approx q$ then $(f^*)'(f'(u))$ is approximately 1 everywhere, and so the original and non-saturating generator gradients are approximately equal, but this is true of any f-divergence. There is no guarantee that the regime $p \approx q$ will ever be approached in the general case where q belongs to a parametric family, and it is not the case that the original and non-saturating generator gradients point in approximately the same direction in general (see §A for an empirical demonstration). In fact, the non-saturating form of generator gradient can have completely different qualitative behavior from the original form. For example, we showed in §3.2 that using the non-saturating variant of the KL generator gradient in fact optimizes reverse KL.

Fedus et al. (2018) argue against the view of GAN training as divergence minimization, based in part on an empirical observation involving the non-saturating scheme. They show (Fedus et al., 2018, Figure 2) that for two well-separated 1D Gaussians, the non-

³In the NIPS paper but not in the arXiv preprint.

saturating GAN loss has a large gradient even for the optimal critic, while Jensen-Shannon has a very small gradient, and use this to argue against viewing non-saturating GAN training as minimizing Jensen-Shannon. The results presented in §2 and §3 show that this set-up computes the gradient of the softened reverse KL, not Jensen-Shannon, and so this observation is not on its own an argument against viewing non-saturating training as divergence minimization.

Arjovsky and Bottou (2017, Section 2.2.2) show that non-saturating GAN training approximately minimizes an objective function. The objective function derived there is expressed as $\text{KL}(q \| p) - 2\text{JS}(p, q)$, which is a rearrangement of the expression $2\text{KL}(\frac{1}{2}p + \frac{1}{2}q \| p)$ derived in §3.2. The paper suggests the negative sign of the second term is “pushing for the distributions to be different, which seems like a fault in the update”, whereas writing the objective function as a divergence makes it clear this is not an issue.

Poole et al. (2016) present a very similar view to that presented in this paper, including recognizing that the generator and critic may be trained to optimize different f-divergences and interpreting classic non-saturating GAN training as a scheme of this form. The divergence derived there can be written as $D_f(p, q) = 2\text{KL}(m \| p) + \text{KL}(p \| m)$ where $m = \frac{1}{2}p + \frac{1}{2}q$ and has $f''(u) = u^{-2} - (1+u)^{-2} = \frac{2u+1}{(1+u)^2 u^2}$. We refer to this as the *improved generator objectives for GANs (IGOG)* divergence. In contrast the softened reverse KL divergence $4\text{KL}(m \| p)$ derived in §3.2 has $f''(u) = \frac{2}{u^2(1+u)}$. We can see from Figure 3 and Table 1 that the IGOG divergence is qualitatively similar to the softened reverse KL derived in this paper, but they are not identical. The discrepancy between the two results is related to matching the value instead of the gradient. In the notation developed in §2.1, Poole et al. (2016, Equation (8)) consider the approximation

$$\mathbb{E}_{x \sim q} [f(p(x)/q(x))] \approx \mathbb{E}_{x \sim q} [f(\exp(d(x)))]$$

and show that for the IGOG divergence the gradient of the right side is equal to the non-saturating generator gradient. This is a valid approximation of the value: for the optimal critic, $d(x) = \log p(x) - \log q(x)$, so the left and right side have the same value. However the gradients are not the same: the partial derivative of the left side with respect to the parameters of q involves two terms, one for each occurrence of $q(x)$, and the partial derivative of the right side only includes one of these. Thus non-saturating GAN training does not minimize the IGOG divergence.

5.4 Practical implications

The focus of this paper is theoretical, but a number of practical implications follow naturally:

- The mode-seeking behavior often observed during non-saturating GAN training is well explained by the softened reverse KL divergence having (2, 0) tail weights. If this is undesirable then using a heavier right tail may encourage diversity.
- Our analysis suggests reverse KL and softened reverse KL are qualitatively similar. Given that reverse KL has a very slightly heavier right tail and better understood theoretical properties, it may make sense to use hybrid (reverse KL, JS) training (§2.2) as a replacement for conventional non-saturating training.
- To monitor progress during non-saturating GAN training, it makes sense to plot the softened reverse KL divergence rather than any other loss. For example, the conventional non-saturating generator loss $-\mathbb{E}_z[\log \sigma(d(g_\lambda(z)))]$ only corresponds to the second term on the right side of (2) and so would not be expected to decrease even if training is progressing well.
- Hybrid training (§2.2) shows that a single critic can be used to approximate any f-divergence. Plotting KL and reverse KL during training helps to monitor mode collapse and sample quality respectively. Pushforward plots are also useful, providing a fine-grained view of the prevalence and severity of mismatches between p and q .
- A critic trained with a symmetric divergence such as Jensen-Shannon will devote equal modelling effort to detecting left and right mismatches, and has the potential to detect mode collapse even if the generator is not able (due to optimization difficulties) or not strongly motivated (due to mode-seeking properties of the f-divergence used) to address it. This will be evident in both the pushforward plot and estimated KL. We provide an example of this in §D.
- The notion of tail weight may be useful for designing new GAN training algorithms. For example, the right tail weight could be annealed from 3/2 to 1 as training progresses. This would encourage diversity and help prevent mode collapse early in training while prioritizing sample quality later in training.

These suggestions for GAN training and avenues for future work are made possible in part by the improved theoretical understanding developed in this paper.

References

- Ali, S. M. and Silvey, S. D. (1966). A general class of coefficients of divergence of one distribution from another. *Journal of the Royal Statistical Society: Series B (Methodological)*, 28(1):131–142.
- Arjovsky, M. and Bottou, L. (2017). Towards principled methods for training generative adversarial networks. In *Proc. ICLR*.
- Arjovsky, M., Chintala, S., and Bottou, L. (2017). Wasserstein generative adversarial networks. In *Proc. ICML*, pages 214–223.
- Balduzzi, D., Racaniere, S., Martens, J., Foerster, J., Tuyls, K., and Graepel, T. (2018). The mechanics of n-player differentiable games. In *Proc. ICML*.
- Bishop, C. M. (2006). *Pattern recognition and machine learning*. Springer.
- Brock, A., Donahue, J., and Simonyan, K. (2018). Large scale GAN training for high fidelity natural image synthesis. In *Proc. ICLR*.
- Cha, S.-H. (2007). Comprehensive survey on distance/similarity measures between probability density functions. *International Journal of Mathematical Models and Methods in Applied Sciences*.
- Csiszár, I. (1967). Information-type measures of difference of probability distributions and indirect observation. *Studia Scientiarum Mathematicarum Hungarica*, 2:229–318. Available at <http://real-j.mtak.hu/id/eprint/5453>.
- Fedus, W., Rosca, M., Lakshminarayanan, B., Dai, A. M., Mohamed, S., and Goodfellow, I. (2018). Many paths to equilibrium: GANs do not need to decrease a divergence at every step. In *Proc. ICLR*.
- Goodfellow, I., Pouget-Abadie, J., Mirza, M., Xu, B., Warde-Farley, D., Ozair, S., Courville, A., and Bengio, Y. (2014). Generative adversarial nets. In *Advances in Neural Information Processing Systems*, pages 2672–2680.
- Grewal, K., Hjelm, R. D., and Bengio, Y. (2017). Variance regularizing adversarial learning. *arXiv preprint arXiv:1707.00309*.
- Gulrajani, I., Ahmed, F., Arjovsky, M., Dumoulin, V., and Courville, A. C. (2017). Improved training of Wasserstein GANs. In *Advances in Neural Information Processing Systems*, pages 5767–5777.
- Karras, T., Aila, T., Laine, S., and Lehtinen, J. (2018). Progressive growing of GANs for improved quality, stability, and variation. In *Proc. ICLR*.
- Karras, T., Laine, S., and Aila, T. (2019). A style-based generator architecture for generative adversarial networks. In *Proceedings of the IEEE Conference on Computer Vision and Pattern Recognition*, pages 4401–4410.
- Kingma, D. P. and Welling, M. (2014). Auto-encoding variational Bayes. In *Proc. ICLR*.
- Kodali, N., Abernethy, J., Hays, J., and Kira, Z. (2017). On convergence and stability of GANs. *arXiv preprint arXiv:1705.07215*.
- Lucic, M., Kurach, K., Michalski, M., Gelly, S., and Bousquet, O. (2018). Are GANs created equal? A large-scale study. In *Advances in neural information processing systems*, pages 700–709.
- Mescheder, L., Geiger, A., and Nowozin, S. (2018). Which training methods for GANs do actually converge? In *Proc. ICML*.
- Mescheder, L., Nowozin, S., and Geiger, A. (2017). The numerics of GANs. In *Advances in Neural Information Processing Systems*, pages 1825–1835.
- Miyato, T., Kataoka, T., Koyama, M., and Yoshida, Y. (2018). Spectral normalization for generative adversarial networks. In *Proc. ICLR*.
- Nagarajan, V. and Kolter, J. Z. (2017). Gradient descent GAN optimization is locally stable. In *Advances in Neural Information Processing Systems*, pages 5585–5595.
- Nowozin, S., Cseke, B., and Tomioka, R. (2016). f-GAN: Training generative neural samplers using variational divergence minimization. In *Advances in Neural Information Processing Systems*, pages 271–279.
- Peng, W., Dai, Y., Zhang, H., and Cheng, L. (2019). Training GANs with centripetal acceleration. *arXiv preprint arXiv:1902.08949*.
- Poole, B., Alemi, A. A., Sohl-Dickstein, J., and Angelova, A. (2016). Improved generator objectives for GANs. In *Proc. NIPS Workshop on Adversarial Training*.
- Reid, M. D. and Williamson, R. C. (2011). Information, divergence and risk for binary experiments. *Journal of Machine Learning Research*, 12(Mar):731–817.
- Sason, I. and Verdú, S. (2016). f-divergence inequalities. *IEEE Transactions on Information Theory*, 62(11):5973–6006.
- Shannon, M. (2020). Properties of f-divergences and f-GAN training. Technical report, Google. Available at <https://arxiv.org/abs/2009.00757>.
- Sønderby, C. K., Caballero, J., Theis, L., Shi, W., and Huszár, F. (2017). Amortised MAP inference for image super-resolution. In *Proc. ICLR*.
- Vajda, I. (1972). On the f-divergence and singularity of probability measures. *Periodica Mathematica Hungarica*, 2(1-4):223–234.
- Vajda, I. (2009). On metric divergences of probability measures. *Kybernetika*, 45(6):885–900.

A Experimental validation

In order to validate our mathematical conclusions we performed GAN training on a simple toy problem where we could explicitly plot the evolution of the generator parameters during training. In this simple set-up it is easy to verify that original, saturating GAN training scheme does indeed converge to a minimum of the Jensen-Shannon divergence and that non-saturating GAN training converges to a minimum of the softened reverse KL divergence.

The details of the experimental set-up were as follows. The true distribution is $p(x) = 0.5\mathcal{N}(x; 0, 0.3^2) + 0.5\mathcal{N}(x; 2, 1)$, a mixture of two 1D Gaussians. The generator is $q(x) = \mathcal{N}(x; \mu, \sigma^2)$ and is parameterized by μ and σ , both set initially to 1.8. The critic architecture in terms of Keras layers is: Dense(20), ELU, Dense(20), ELU, Dense(1). We also tried training using the analytically optimal critic, which is equivalent to SGD on the divergence value. GAN training was performed using vanilla stochastic gradient descent. In all cases the critic was trained using the canonicalized Jensen-Shannon divergence (learning rate $2 \cdot 10^{-2}$). The generator was trained with canonicalized Jensen-Shannon (learning rate $4 \cdot 10^{-3}$) as well as the conventional non-saturating generator loss multiplied by two (to make it precisely equivalent to softened reverse KL), reverse KL and the canonicalized IGOG divergence (all using a learning rate of $2 \cdot 10^{-3}$). A batch size of 256 was used. The critic was updated 5 times between each generator step (alternating SGD). Training proceeded for 4000 generator updates.

The evolution of the generator parameters during training is shown in Figure 5. In all cases, training approximately converges to a minimum of the corresponding divergence value as expected based on the theoretical arguments presented in the main body.

B Divergence boundedness

Some f-divergences such as Jensen-Shannon are bounded, while others such as KL are unbounded. This is relevant for training since we might expect bounded divergences to have weak gradients when starting from a random initialization. In this section we provide a characterization of the boundedness of D_f in terms of the behavior of $f(u)$ for small and large u , following Vajda (1972). This will be related to tail weight in the next section.

Given an f-divergence D_f , define:

$$M = \sup_{p,q} D_f(p, q) \quad (16)$$

$$M_0 = \sup_{u \in (0,1)} f(u) \quad (17)$$

$$M_\infty = \sup_{u > 1} \frac{f(u)}{u} = \sup_{u \in (0,1)} f_R(u) \quad (18)$$

The supremums are guaranteed to exist but may be infinite. Vajda (1972, Theorem 2, “range of values”) showed that

$$M = M_0 + M_\infty \quad (19)$$

We refer to a divergence as *left-bounded* if $M_0 < \infty$, *right-bounded* if $M_\infty < \infty$, and *bounded* if $M < \infty$. Thus a divergence is bounded iff it is left-bounded and right-bounded.

We briefly describe how to establish (19). It is straightforward to see that $M \leq M_0 + M_\infty$: on the right side of (10), the first term has $f(u) \leq M_0$ and the second term has $f_R(u^{-1}) \leq M_\infty$, so $D_f(p, q) \leq M_0 + M_\infty$ as desired. For the converse direction, we need to exhibit probability distributions p and q with $D_f(p, q)$ arbitrarily close to $M_0 + M_\infty$. This is most straightforward in the case where p and q are distributions over the two-point set $\{0, 1\}$. Given $r, s \in (0, 1)$, let $p_r(0) = r$ and $q_s(0) = s$. This determines p_r and q_s entirely, and we have

$$D_f(p_r, q_s) = sf\left(\frac{r}{s}\right) + (1-r)f_R\left(\frac{1-s}{1-r}\right) \quad (20)$$

Now a defining function f is monotonically decreasing on $(0, 1)$, so we can replace the supremum in (17) with a limit: $f(u) \rightarrow M_0$ as $u \rightarrow 0$. Thus as $r \rightarrow 0$ and $s \rightarrow 1$, $D_f(p_r, q_s) \rightarrow M_0 + M_\infty$ as desired. For the continuous case where p and q are densities over \mathbb{R}^K , we reduce this to the discrete case by considering mixtures of Gaussians with shrinking covariances. Fix any two distinct points $\mu_0, \mu_1 \in \mathbb{R}^K$. Let $\tilde{p}_{r\sigma}(x) = r\mathcal{N}(x; \mu_0, \sigma^2 I) +$

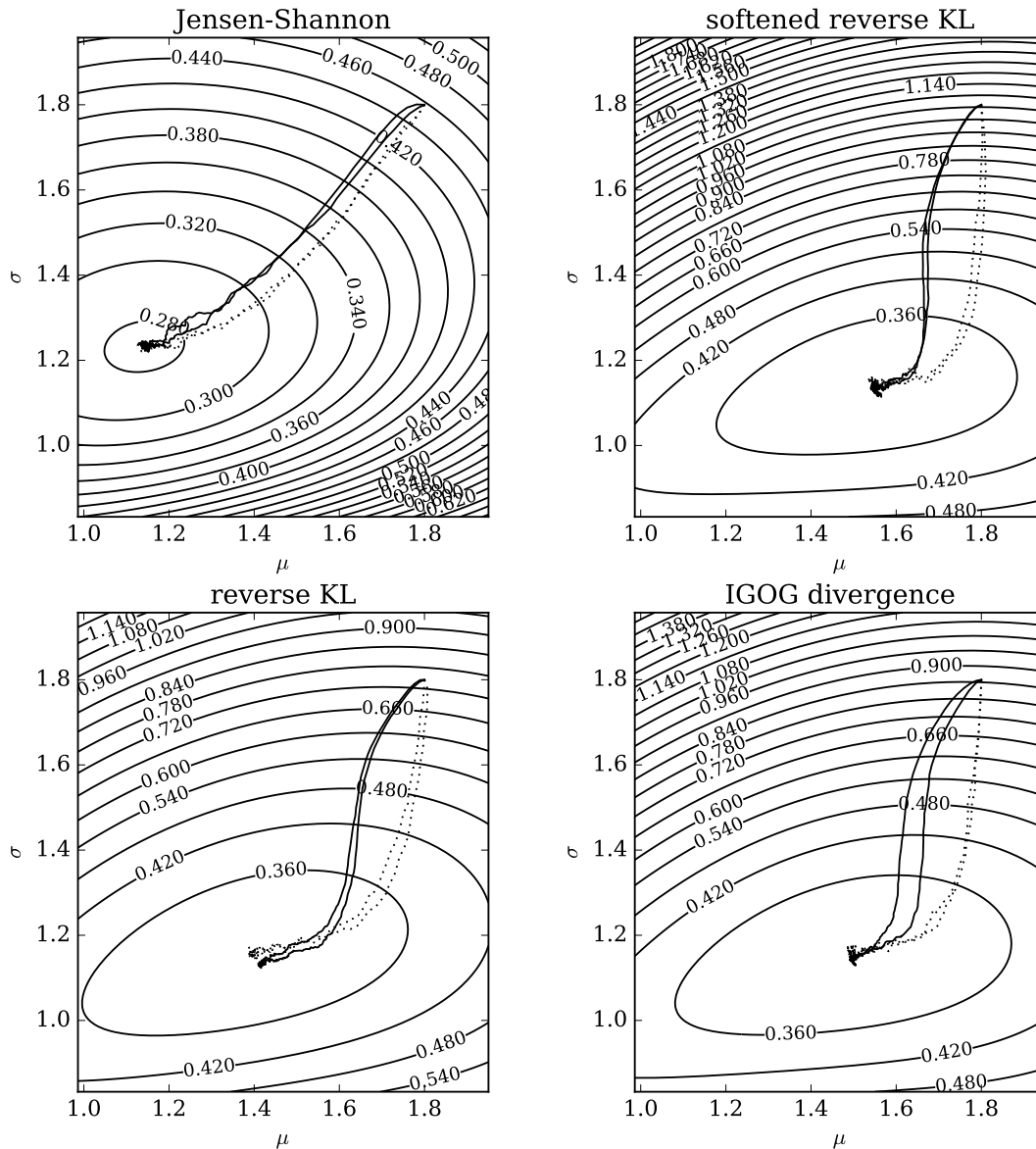


Figure 5: Comparing training using the saturating and non-saturating GAN generator gradient on a toy problem. The true distribution p is a mixture of two 1D Gaussians and the model distribution q is a single Gaussian. Contour plots show the values of various divergences considered in this paper as a function of the generator parameters μ and σ . Lines show the progression of SGD-based GAN training using the original, saturating GAN training scheme (Jensen-Shannon panel), non-saturating GAN training (softened reverse KL panel), and hybrid (reverse KL, Jensen-Shannon) and (IGOG divergence, Jensen-Shannon) training schemes (bottom two panels). The solid lines show two independent training runs with a learned critic. The dotted lines show two independent training runs with the analytically optimal critic. Training approximately converges to the expected divergence minimum in all cases.

$(1-r)\mathcal{N}(x; \mu_1, \sigma^2 I)$ and $\tilde{q}_{s\sigma}(x) = s\mathcal{N}(x; \mu_0, \sigma^2 I) + (1-s)\mathcal{N}(x; \mu_1, \sigma^2 I)$ where $r, s \in (0, 1)$ as before. As $\sigma \rightarrow 0$, $D_f(\tilde{p}_{r\sigma}, \tilde{q}_{s\sigma}) \rightarrow D_f(p_r, q_s)$. Given $\varepsilon > 0$, we can find $r, s \in (0, 1)$ such that $D_f(p_r, q_s)$ is within ε of $M_0 + M_\infty$, and given this r, s we can find $\sigma > 0$ such that $D_f(\tilde{p}_{r\sigma}, \tilde{q}_{s\sigma})$ is within ε of $D_f(p_r, q_s)$. Thus $D_f(\tilde{p}_{r\sigma}, \tilde{q}_{s\sigma})$ is within 2ε of $M_0 + M_\infty$. Thus there exist continuous probability distributions with divergence value arbitrarily close to $M_0 + M_\infty$.

C Tail weight properties and computation

In this section we provide more details on tail weights. We describe the relationship between boundedness and tail weights and provide some examples of how tail weights may be computed.

Tail weight determines boundedness. It can be checked by integrating and bounding that a divergence with (L, R) tail weights is left-bounded iff $L < 2$ and right-bounded iff $R < 2$. Thus D_f is bounded iff $L, R < 2$. Boundedness properties can also be seen in Figure 2. Left and right boundedness of D_f is equivalent to left and right boundedness of s_f . Thus we can see that reverse KL is left-unbounded but right-bounded, for example.

Tail weights also interact in a simple and intuitive way with linearity: if one f-divergence has (L_1, R_1) tail weights and another has (L_2, R_2) tail weights then their sum has $(\max_i L_i, \max_i R_i)$ tail weights.

Tail weights are relatively straightforward to compute for a given f-divergence. The definition from §4.3 is that D_f has left tail weight L if $f''(u) \sim Cu^{-L}$ as $u \rightarrow 0$ for some $C \in \mathbb{R}$. Here \sim may be read as “is asymptotic to” and “ $g(u) \sim h(u)$ as $u \rightarrow a$ ” has the meaning “ $g(u)/h(u) \rightarrow 1$ as $u \rightarrow a$ ”. Thus D_f has left tail weight L iff $u^L f''(u)$ tends to a constant as u tends to zero. The general idea for computing left tail weight is therefore to work out what power of u we need to multiply $f''(u)$ by in order for it to tend to a constant as u tends to zero. The \sim notation makes this a little easier since we can make use of two properties: if $f(u) \sim g(u)$ and $g(u) \sim h(u)$ as $u \rightarrow a$ then $f(u) \sim h(u)$; and if $f_1(u) \sim g_1(u)$ and $f_2(u) \sim g_2(u)$ as $u \rightarrow a$ then $f_1(u)f_2(u) \sim g_1(u)g_2(u)$. For example, Jensen-Shannon has $f''(u) = \frac{2}{u(1+u)}$. As $u \rightarrow 0$, we have $\frac{2}{1+u} \rightarrow 2$, and so $\frac{2}{1+u} \sim 2$, and so $f''(u) \sim 2u^{-1}$, and so the left tail weight is 1. For the softened reverse KL, $f''(u) = \frac{2}{u^2(1+u)}$, so in the same way we see that $f''(u) \sim 2u^{-2}$ and so the left tail weight is 2. The right tail weight is defined as R if $f''(u) \sim Du^{R-3}$ as $u \rightarrow \infty$ for some $D \in \mathbb{R}$. For example, for Jensen-Shannon we can multiply the top and bottom by u to obtain $f''(u) = \frac{2u}{u^2(1+u)}$, and $\frac{u}{1+u} \rightarrow 1$ as $u \rightarrow \infty$, so $f''(u) \sim 2u^{-2}$, so $R - 3 = -2$, so $R = 1$. Alternatively we can replace u by u^{-1} and seek the asymptotic behavior as $u \rightarrow 0$.

D Examples of pushforward plots

In this section we show some examples of pushforward plots for a variety of learned generators. This is intended to provide a more intuitive understanding of what pushforward plots capture, as well as the ways in which they might be useful for monitoring training.

Figure 6 and Figure 7 show mode-seeking and covering behavior for a model trained with reverse KL and KL respectively. Here the model mismatch comes from the generator using a diagonal covariance while the data is generated from a full covariance Gaussian with strong correlation between the two dimensions. Figure 8 and Figure 9 show similar behavior for a “circle of Gaussians” example. Here the mismatch comes from the true distribution being a mixture while the generator is unimodal. Figure 10 shows an example of mode collapse for a generator trained on MNIST digits. It is interesting to note that the critic is able to accurately detect the mode collapse, even though the generator training has not been able / motivated to use this information to remedy the problem.

E Divergence symmetrization and softening

In this section we describe three simple operations that can be applied to an divergence to obtain another divergence: reversing, symmetrizing and *softening*. Many common f-divergences can be obtained from others in this way. For example, all the f-divergences considered in this paper can be obtained by applying these operations to the KL divergence. We refer to $4\text{KL}(\frac{1}{2}p + \frac{1}{2}q \| p)$ as the *softened reverse KL divergence* because it may be obtained by applying the softening operation to the reverse KL.

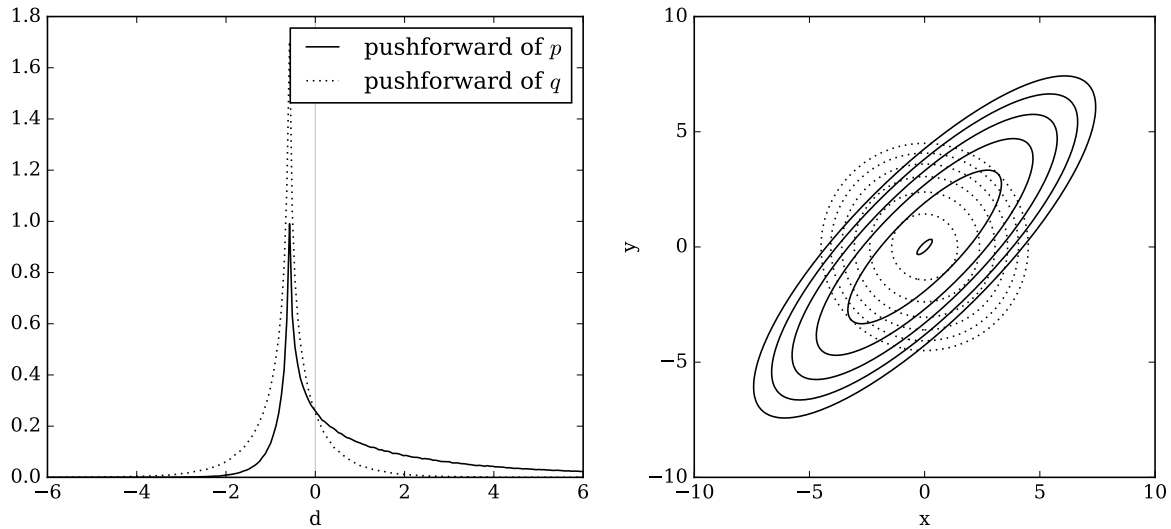


Figure 6: Plots of the pushforward densities $\tilde{p}(d)$ and $\tilde{q}(d)$ for the case where p is a 2D Gaussian with covariance $[[5.5, 4.5], [4.5, 5.5]]$ and q is a diagonal covariance model fit with reverse KL. We can see from the heaviness of the tails that there are substantial right mismatches and that q is more compact than p . A contour plot of the data-space density of p and q is also shown.

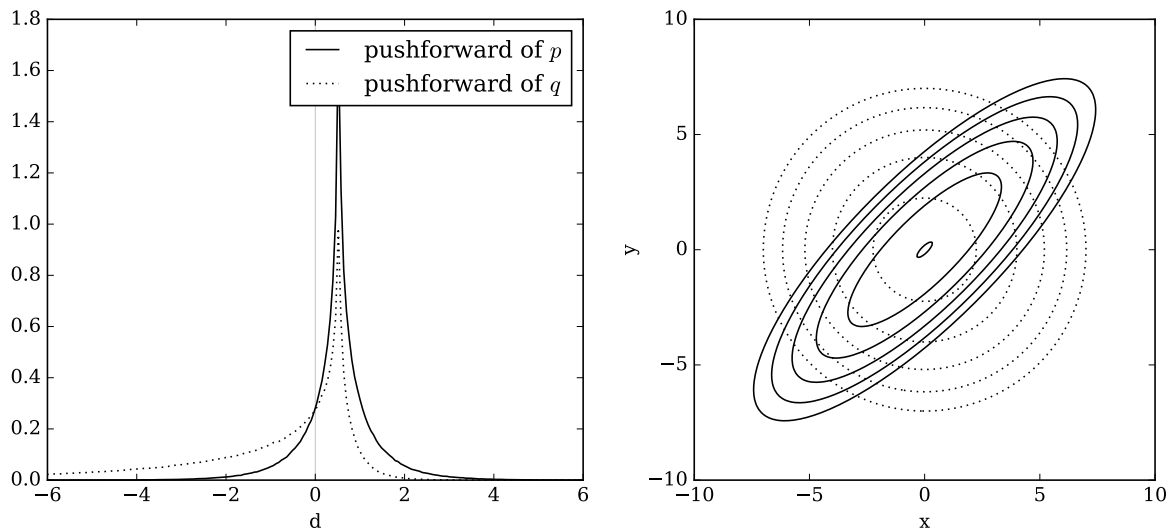


Figure 7: The analogue of Figure 7 for KL instead of reverse KL. We can see from the heaviness of the tails that there are substantial left mismatches and that q is broader than p (covering behavior).

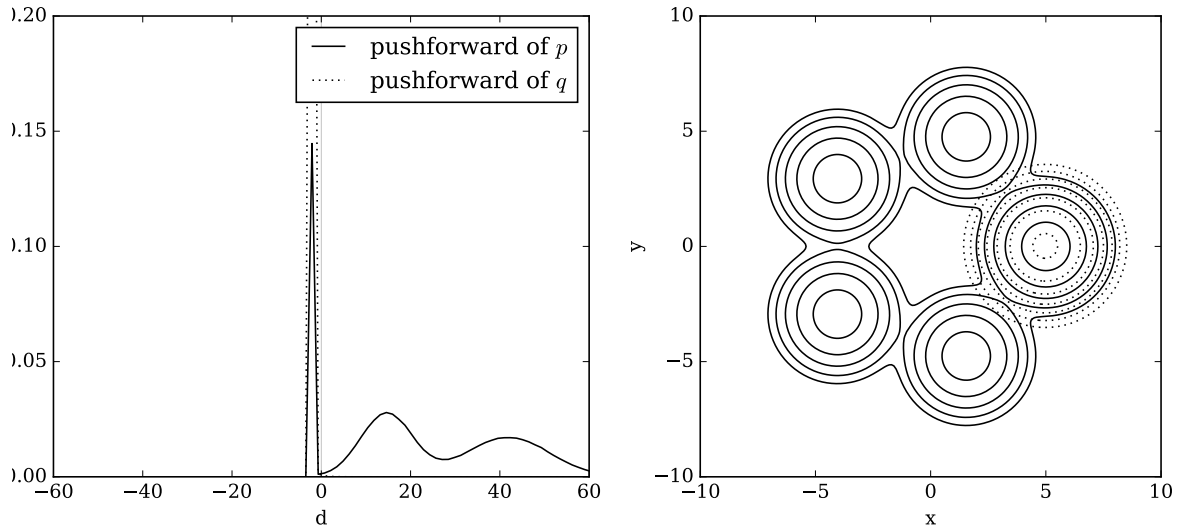


Figure 8: Plots of the pushforward densities $\tilde{p}(d)$ and $\tilde{q}(d)$ for the case where p is a 2D mixture of five Gaussians with means arranged in a circle at radius 5 from the origin and identity covariance matrices and q is an isotropic Gaussian with mean and scale fit using reverse KL. This is a prototypical example of mode collapse. We can actually see the modes which are being dropped in the pushforward plot: there is one peak in $\tilde{p}(d)$ for the two nearer dropped modes and one peak for the two further dropped modes. Note the wider scale of d . A contour plot of the data-space density of p and q is also shown.

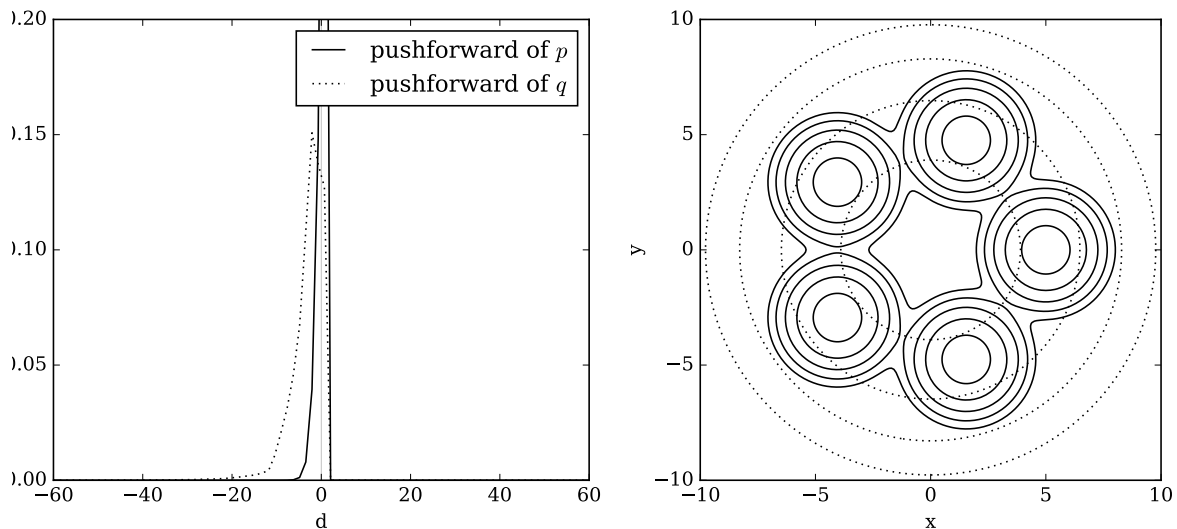


Figure 9: The analogue of Figure 9 for KL instead of reverse KL. We can see the covering behavior in the pushforward plot by the relatively strong left tail of $\tilde{q}(d)$, though in this case the left mismatches caused by fitting with KL are less extreme than the right mismatches caused by fitting with reverse KL.

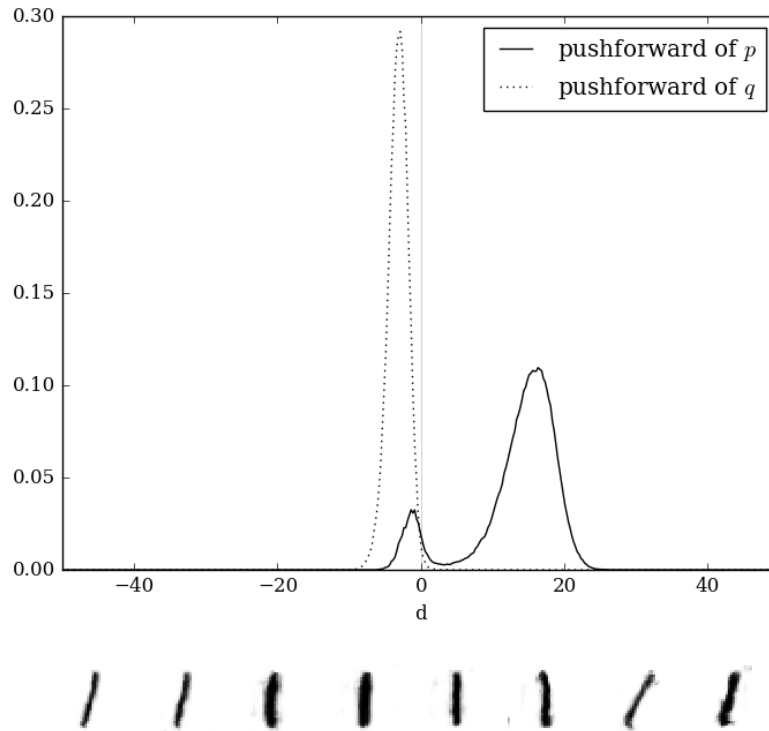


Figure 10: Example of a pushforward plot demonstrating mode collapse on a real dataset. Samples from the generator are shown below the pushforward plot. The generator has a StyleGAN-like architecture and was trained on MNIST digits using a hybrid (reverse KL, Jensen-Shannon) training scheme. The generator output lacks diversity, consisting of various forms of the digit 1. This is evidenced by a large right mismatch in the pushforward plot representing the nine other digits which have extremely low probability of being produced by the generator. Here the learned critic rather than the optimal critic is used for the pushforward. It is interesting to note that the critic has learned to detect the mode collapse (that is, learned to assign a score indicating a large mismatch to natural images of the other nine digits), even though the generator training has not been able to use this information effectively, presumably due to optimization difficulties and the use of a divergence which does not penalize right mismatches heavily.

Consider applying an operation to a divergence D to obtain another divergence \tilde{D} . If this operation maps f-divergences to f-divergences then we may also think of it as mapping a defining function f to another defining function \tilde{f} . We already saw the reversing operation $D \mapsto \tilde{D}$ where $\tilde{D}(p, q) = D(q, p)$ in §4.1. This has $\tilde{f} = f_{\text{R}}$ where $f_{\text{R}}(u) = uf(u^{-1})$. In this case

$$\tilde{f}''(u) = f_{\text{R}}''(u) = u^{-3} f''(u^{-1}) \quad (21)$$

and $a_{f_{\text{R}}}(d) = -b_f(-d)$ and $b_{f_{\text{R}}}(d) = -a_f(-d)$ as might be expected intuitively. Symmetrization means $\tilde{D}(p, q) = \frac{1}{2}D(p, q) + \frac{1}{2}D(q, p)$. This has $\tilde{f} = \frac{1}{2}f + \frac{1}{2}f_{\text{R}}$ and

$$\tilde{f}''(u) = \frac{1}{2}f''(u) + \frac{1}{2}f_{\text{R}}''(u) \quad (22)$$

We define (q -)softening as replacing q with $m = \frac{1}{2}p + \frac{1}{2}q$, i.e. $\tilde{D}(p, q) = 4D(p, m)$. This has $\tilde{f}(u) = 2(1+u)f(\frac{2u}{1+u})$ and

$$\tilde{f}''(u) = \frac{8}{(1+u)^3} f''\left(\frac{2u}{1+u}\right) \quad (23)$$

The factor of 4 in the definition of \tilde{D} ensures that a softened canonical divergence remains canonical. Softening has the potential to make large right mismatches much less severely penalized, since in regions of space where $p(x)/q(x)$ was large because $p(x)$ was moderate and $q(x)$ was tiny, $p(x)/m(x)$ is now approximately 2, so a large right mismatch is only penalized by the softened divergence as much as a moderate right mismatch is penalized by the original divergence. This is reflected in the tail weights: It is easy to show using the tools we have developed above that if the original divergence has (L, R) tail weights then the softened divergence has $(L, 0)$ tail weights. For completeness, we could also define p -softening as replacing p with $m = \frac{1}{2}p + \frac{1}{2}q$, i.e. $\tilde{D}(p, q) = 4D(m, q)$. This has $\tilde{f}(u) = 4f(\frac{1}{2}(1+u))$ and

$$\tilde{f}''(u) = f''\left(\frac{1}{2}(1+u)\right) \quad (24)$$

If D_f has (L, R) tail weights then the p -softened divergence has $(0, R)$ tail weights. Softening was considered by Vajda (2009, Equations (41) and (42)), where it was referred to as *normalization*.

Many f-divergences can be written concisely as a series of these operations. For example reverse KL is Reverse(KL), Jeffreys is Symmetrize(KL), the canonicalized K-divergence $4\text{KL}(p \parallel m)$ (Cha, 2007) is Soften(KL) and canonicalized Jensen-Shannon is Symmetrize(Soften(KL)). The softened reverse KL divergence $4\text{KL}(m \parallel p)$ that is the focus of this paper is Soften(Reverse(KL)).